

Rising obstacle in a one-layer granular bed induced by continuous vibrations: two dynamical regimes governed by vibration velocity

Hui Zee Then, Teruyo Sekiguchi, and Ko Okumura

Physics Department and Soft Matter Center, Ochanomizu University, Japan

(Dated: November 4, 2021)

Abstract

Rising motion of an obstacle in a vibrated granular medium is a classic problem of granular segregation, and called the Brazil nut (BN) effect. The controlling vibration parameters of the effect has been a long-standing problem. A simple possibility that the BN effect can be characterized solely by vibration velocity has recently been pointed out. The issue has become controversial before a long history of research, with only a few systems have provided for the simple possibility. Here, we investigate the rising motion of an obstacle in a vertically positioned one-layer granular bed under continuous vibrations. We find the rising motion is composed of two distinct regimes, and the first and second regimes are both governed, in terms of vibration parameters, solely by the vibration velocity. We further demonstrate simple scaling laws well describe the two regimes. Our results support the emergent possibility on the controlling parameters of the BN effect and suggests that this feature would be universal. We propose two possible mechanisms of convection and arch effect for the two distinct regimes and demonstrate these mechanism explain the scaling laws followed by our experimental data.

I. INTRODUCTION

When a cell that contains mixture of grains of large and small sizes are vibrated, large ones tend to rise up in the cell. This effect is a typical example of size segregation of grains by shaking, known as the Brazil nut (BN) effect [1, 2]. Since pioneering studies in simulation [3] and experiments [4–6], many studies have been performed in the field of physics. As a result a number of physical mechanisms of the phenomenon have been proposed, which include void filling [7], convection [5], and arching effect [6].

However, as for the controlling vibration parameters of the BN effects, our understanding has become controversial. It has been believed that the characterization of the convection-driven rising motion requires at least two vibration parameters, the acceleration and frequency [8, 9]. However, several years ago, it was clearly shown that the convection-driven rising motion is characterized, in terms of vibration parameters, solely by the vibration velocity, in a wide range of experimental parameters [10]. Subsequently, a detailed study on the granular convection induced by vibration revealed that the convection velocity is well characterized by the velocity [11], supporting the recent study [10]. However, despite a long history of research, the vibration-velocity governed BN effect has been reported only in a few cases [10, 12], and the problem of controlling vibration parameters has become controversial (e.g., well-known MRI studies [8, 13] did not demonstrate their data can be characterized solely by vibration velocity). Therefore, providing experimental data that can be characterized solely by vibration velocity in different systems is an emergent important issue for settling this long-standing issue.

In order to elucidate the controlling vibration parameters in the BN effect, we investigate the rising motion in a one-layer granular bed under continuous vibration. As a result, we find that the dynamics are divided in first and second regimes, and both are well characterized solely by the vibration velocity through simple scaling laws. In addition, we propose possible mechanisms of convection and arch effect for the two regimes, and demonstrate these mechanisms explain the scaling laws followed by the experimental data.

II. EXPERIMENT

The setup is shown in Fig. 1a. A cell of thickness 1.2 mm was filled with beads of average diameter 1.0 mm and a stainless-steel disk of thickness 1.0 mm. The cell is mounted on a vibration system, which causes rising motion of the disk in granular medium (consisting of one layer of beads) with the disk sliding freely on the side in the medium.

We used a cell with side walls slightly down-facing with an angle about 5 degrees (specified below) throughout this study. Slight side-wall angle was necessary to observe stable rising motion of the disk. When the side walls were vertical, the rising motion was not smooth and not well-reproducible. Dependence on the angle may originate from a weak friction on the side walls and a relatively weak polydispersity of our beads (the bead diameter were approximately in the range 0.9-1.15 mm), which tends to create lattice structures. With a slight down-facing angle, lattice structures tend to be broken and the movement of beads near the side walls are restrained as in the case when friction on the side wall is strong. Note that the importance of friction on the vertical side wall for convection was pointed out [5]. They also demonstrated that the introduction an angle in the opposite up-facing direction can reverse the direction of convection. However, in the present case, the angle was smaller and introduced to conduct reproducible study of the BN effect. In this sense, the slight side-wall angle could be considered as a substitute for polydispersity and friction near the side walls.

A cell of thickness $t = 1.2$ mm was made from two transparent acrylic plates of thickness 3 mm, separated with spacers of thickness t . The cell height H was fixed to 140 mm. The top and bottom widths of the cell, W_1 and W_2 (see Fig. 1a), were slightly different with a finite angle α defined by $\tan \alpha = (W_2 - W_1)/(2H)$. The width of the cell W was defined as $W = (W_1 + W_2)/2$ for convenience. The cell width W was either 55, 80, 85, or 105 mm. In the case of $W = 85$ mm, W_1 and W_2 were set to $W_1 = 80$ and $W_2 = 90$ mm, while W_1 and W_2 for different W were determined such that the angle α was the same with that for $W = 85$ mm, i.e., α was fixed to a value $\alpha = \arctan[(90 - 80)/(2 \cdot 140)]$ (~ 5 degrees).

The cell contained a disk-shaped obstacle (diameter $D = 12, 15,$ or 18 mm and thickness 1 mm) and one layer of small balls of aluminum oxide with an average diameter $d = 1$ mm (AL-9, AS ONE Corp.). The balls filled the cell with the obstacle to a depth $h = 100$ mm. The density of disks ($7.7 - 7.9$ g/cm³) are larger than that of small alumina balls (3.95

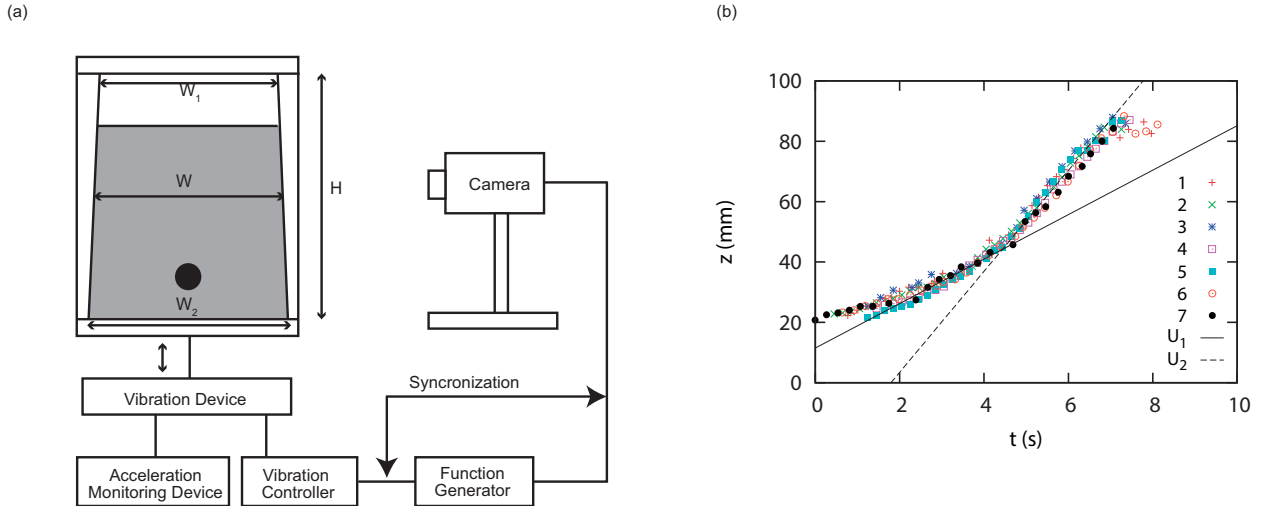


FIG. 1: (a) Experimental setup. The bottom of the vertically-positioned cell is set as the bottom of the vertical axis z . (b) The position z of the intruder as a function of time t for the cell with $W = 85$ mm and the intruder with $D = 12$ mm at the frequency $f = 30$ Hz and the vibration acceleration $a = 50$ m/s². The ascent of the intruder proceeds with two stages. The smaller and larger slopes indicated by the lines respectively characterize the corresponding two velocities U_1 and U_2 . See the text for the details.

g/cm³).

The cell containing the obstacle and grains was mounted vertically on a vibration generator system (m060/MA1-CE, IMV Corp.), which was controlled by a multi-function generator (WF1948, NF Corp.) and monitored by an acceleration meter (VM-1970, IMV Corp.). Digital images were obtained with a CCD camera (STC-MB33USB, SENTECH Co., Ltd.), which was synchronized with the vibration system through the function generator.

The vibration generation system can produce continuous sinusoidal waves with a control on the angular frequency ω and amplitude A . The sinusoidal wave can be characterized by the vibration velocity $v = \omega A$, acceleration $a = \omega^2 A$, and frequency $f = \omega/(2\pi)$.

III. RESULTS

A. Rising motion

As shown in Fig. 1b, the intruder rises in the layer of grains with time under vibration. The different symbols correspond to different ascent experiments performed under the same condition specified in the caption. As seen in the plot, all the data points collapse onto a master curve except near the starting point, demonstrating a reasonable reproducibility of the experiment. The master curve can be divided into two regimes, characterized by two velocities U_1 and U_2 , as indicated in the plot. The linearity in the second region was more visible than in the first. Determination of the slopes corresponding U_1 and U_2 is explained below in detail. The crossover depth was around 40 to 60 mm in our parameter ranges, but it was not sensitive to parameter changes (it was difficult to find a systematic trend). The initial position was set to $z = 20$ mm. When the intruder was initially placed at a deeper position, the rising motion of the disk became less reproducible near the bottom. A critical initial depth for rising was difficult to define because it seemed to be dependent on uncontrollable initial configurations of beads.

B. Simple laws for U_1 and U_2

Figure 2 a and b show the two velocities U_1 and U_2 obtained under various conditions as a function of the vibration acceleration a . As demonstrated in Fig. 2 c and d, after carefully looking dependence of the data on experimental parameters, we found that the data can be well described by the relations

$$\frac{U_1}{\sqrt{gd}} = k_1 \frac{v^2}{Wg} \quad (1)$$

$$\frac{U_2}{v_c} = k_2 \frac{D(v - v_c)}{Wv_c} \quad (2)$$

where g is the gravitational acceleration with $v_c = 126 \pm 5$ mm/s, $k_1 = 0.88 \pm 0.022$ and $k_2 = 0.85 \pm 0.016$. The fitting parameter v_c was introduced because in the U_1 vs v plot the data were well on a straight line and the line intersects with the v axis at the same point (within experimental errors), irrespective of D and W . Note v_c is of the same order of \sqrt{gd} , which is a natural velocity scale in the present problem, as appears in Eq. (1).

The following information could be gleaned from the values of k_1 and k_2 . (I) The fact that k_1 and k_2 are both close to one confirms that the order of magnitudes predicted by Eqs. (1) and (2) are consistent with our experimental data. (II) The fact that the standard deviations for k_1 and k_2 thus obtained are less than a few per cent (they are 2.51 and 1.85 %, respectively) suggests that our experimental data and their analysis are of high quality.

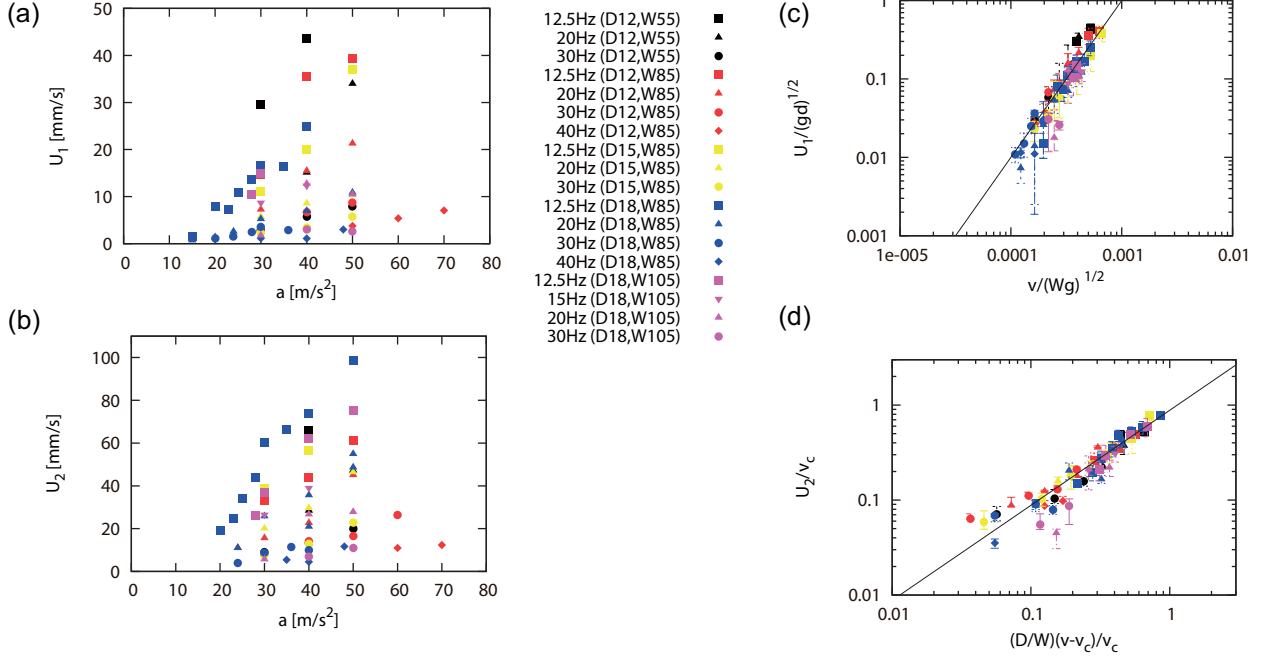


FIG. 2: (a) and (b): The rising velocity in the first regime U_1 and that in the second regime as a function of the vibration acceleration a for different vibration frequencies, 12.5 Hz (squares), 20 Hz (triangles), 30 Hz (circles) and 40 Hz (diamonds). Data for $(D, W) = (12, 55)$, $(12, 85)$, $(15, 85)$, $(18, 85)$ and $(18, 105)$ are represented by black, red, yellow, blue, magenta symbols, respectively. (c) All the data in (a) replotted with renormalized axes. The line with a slope 2 represents Eq. (1) with $k_1 = 0.88 \pm 0.022$. (d) All the data in (b) replotted with renormalized axes. The line with a slope 1 represents Eq. (2) with $k_2 = 0.85 \pm 0.016$.

Details of obtaining values and error bars for Fig. 2 c and d are explained as follows. We prepared n sets of data under the same experimental condition, i.e., for a set of (D, W, f, v) . For each set of data, we first determined the second region exploiting its clear linearity with a slope (corresponding to U_2), and the data in the remaining region was fit by a straight line with another slope (corresponding to U_1). This second fit was conducted by selecting a linear region as wide as possible with the criterion that the coefficient of determination

became below 0.98 (this coefficient was determined by $1 - \sum_{i=1}^m (z_i - z_P)^2 / \sum_{i=1}^m (z_i - z_A)^2$ where z_P and z_A are the predicted and average values, respectively, for m data of z_i). This well-defined method to determine U_1 was used based on the following observations. (1) Rising motion was unstable near the starting point with less reproducibility. (2) However, before the second region, which is clearly linear, another linear region tended to appear and its slope was well reproducible although its width was not. These features are visible in Fig. 1 b if compares the slopes and the experimental data. Note that k_1 and k_2 used in Fig. 1b are the same values obtained from Fig. 2c and d. In this way, we obtained n different sets of (U_1, U_2) for a single set of (D, W, f, v) . If n was larger than 10 we employed the standard deviation for the error bar. Otherwise, the highest and lowest positions of the error bar were determined by the maximum and minimum values, respectively.

IV. PHYSICAL INTERPRETATIONS

A. First regime: ascent by filling of an arch-shaped void created

The physical mechanism for rising in the first regime can be considered as a result of filling by small beads of an arch-shaped void created at the bottom of the cell during vibration as illustrated in Fig. 3 a. These arch shapes are created as a result of time-sequential motion as shown in Fig. 3 b.

For simplicity, we consider the case $a \gg g$ to gain physical insight into this sequential motion (In fact, the ascent can be observed only when $a > g$, as also reported in [10, 14]). When a sinusoidal wave is applied to the system, the normal force acting on the system of one grain layer and the intruder (total mass M) from the cell bottom is given by $N = -Mg - M\alpha$, as long as the system holds contact with the cell bottom, if we neglect the friction effect near the side walls. Here, $\alpha = -a \cos \omega t$ is the acceleration corresponding to the movement of the position of the base plate of the cell described by $z = A \cos \omega t$. This means, when $a \gg g$, soon after the cell moves upwards from the central position of vibration, $z = 0$, the normal N becomes zero and the system starts a parabolic motion under gravity with the initial speed comparable to $v = \omega A$. The maximum height of the parabolic motion scales as h with $v^2 \simeq gh$ (this relation is exact in Newtonian mechanics, in the absence of side walls with the constraint that all the particles are on the vertical plane, and thus tends to

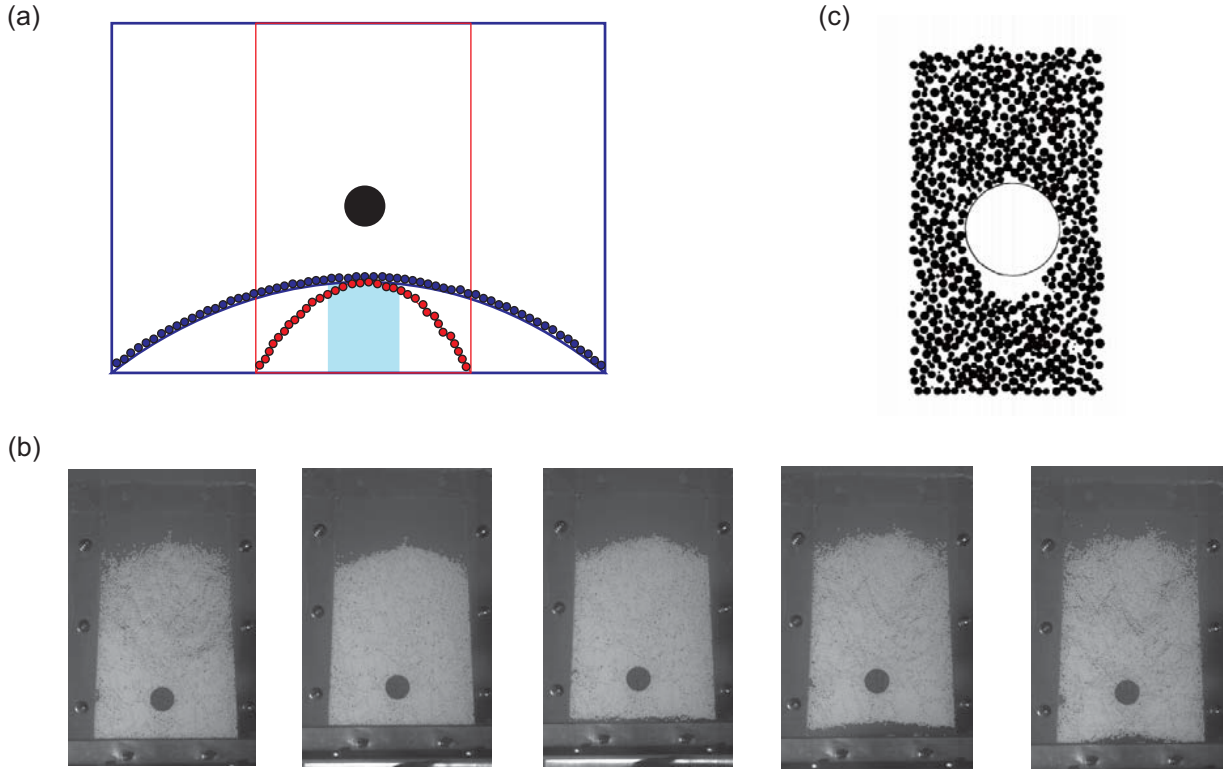


FIG. 3: (a) Illustration of two arches repeatedly formed at the bottom of the layer during vibration, one in a cell with a wider cell and another with narrower cell. The width of the arch is determined by the side walls of the cell. This illustration superimposes two cases, a wider cell and a narrower cell at the same vibration velocity when the arch becomes most significant (such a moment repeatedly appear with a given frequency). The height at the center is the same for the two cells because it is set by v^2/g as explained in the text. (b) Sequential snapshots, separated by 10 ms, of a cell of $W = 85$ mm under vibration at $f = 12.5$ Hz and $a = 30$ mm/s² with an intruder of $D = 15$ mm. The arch-shaped void is created at the bottom of the granular layer, which is most visible in the second right-most photograph. (c) Void filling mechanism suggested in previous studies: black particles continuously fill up the void created beneath the intruder during shaking, which results in the rising of the intruder. (c) is reproduced from Ref. [7] (Copyright, APS 1992).

hold in the central region if the wall distance is large and friction with front and back walls is small, which is the present case). When $a \gg g$, the maximum height h is considerably larger than the vibration amplitude A , and in such a case the maximum height of the layer bottom relative to the cell bottom is comparable to h , which is the same under a fixed v .

However, small beads close to the side walls cannot move (relative to the cell) because

of the friction effect near the side walls, while small beads around the center of the cell repeatedly go up with the intruder under vibration till the maximum height comparable to $h \simeq v^2/g$ (relative to the cell bottom) as estimated as above. This leads to the formation of a velocity gradient in the granular layer in the direction of cell width, which results in an arch-shaped void at the bottom of the layer as shown by the snapshots in Fig. 3 b. During the formation of an arch-shaped void, some beads close to the bottom of the layer enter into the void due to the velocity gradient, which results in a shear force. As a result, the height of the intruder relative to the cell bottom when it is next pushed to the cell bottom becomes higher than before. This is the mechanism of ascent by void filling.

This mechanism of the ascent by void filling is consistent with the dependence of the ascent velocity U_1 on the cell width W and on the vibration velocity v , predicted in Eq. (1). As long as $a \gg g$, for a fixed v , the maximum height of the arch comparable to h given above is the same, meaning that the velocity gradient increases as W decreases. Accordingly, we expect that U_1 increases as W decreases, which qualitatively explains why U_1 scales with $1/W_1$ in Eq. (1). For a fixed W , because h scales with v^2 , if the void were completely filled, U_1 would scale with ωv^2 by noting that the period of vibration scales as $1/\omega$. However, the void filling is much less effective, as observed in Fig. 3 b. Since the effectiveness increases with the period $\simeq 1/\omega$, we expect the ascent per vibration may scale not with ωv^2 but this factor multiplied with the effectiveness factor $1/\omega$, which results in U_1 scaling with v^2 , in accordance with Eq. (1). Note that the number of beads falling off from the arch will increase as the life time of the transient arch increases, i.e., the period of vibration increases (as shear tends to increase the number). In this sense, the effectiveness of void filling increases with $1/\omega$ (as W decreases the effectiveness reducing shear).

According to Eq. (1), U_1 is independent of the disk diameter D . This is in contrast with the ascent ascribed to void filling mechanism in the previous studies [2, 3, 7]. The void considered in the previous studies is not the arch-shaped void but a void formed beneath the disk as illustrated in Fig. 3 b. This implies the ascent velocity increases with D . However, in the present case, the size of the arch-shaped void is independent of the size of the disk (this is because the width is set by W and the height is set by v^2/g as explained above), and, thus, it is natural that U_1 is independent of D .

B. Second regime: ascent by convection

The physical mechanism for rising in the second regime can be considered as a result of convection. To draw this conclusion, we put a steel bead (silver color) of the same diameter (1 mm) in a layer of alumina beads (white color) and track the movement of the steel bead (density 7.85 g/cm^3). As seen in a typical result, shown in Fig. 4 a, a convective roll motion is observed in the right side of the cell. By analyzing the chronological order of black dots corresponding to the steel bead, it is revealed that the flow is upward in the center of the cell and is downward near the wall. From symmetry, a similar roll should exist in the left side of the cell. The upward flow near the center starts at a certain height where two flows merge, one from the right side and the other from the left side, and this height seems to correspond to the height of the transition from the first regime characterized by U_1 to the second by U_2 . Accordingly, we can expect that the rising motion in the second regime is due to the convective roll motion.

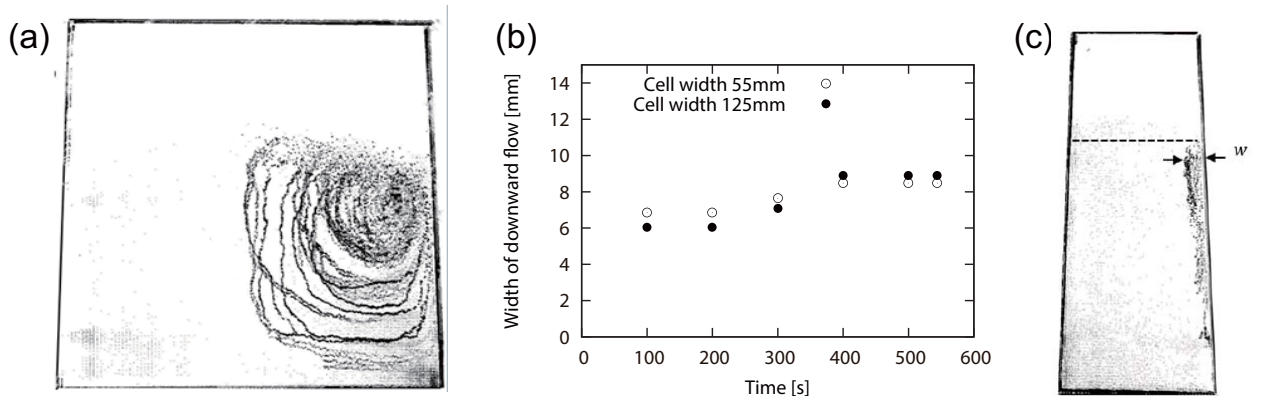


FIG. 4: (a) Convection roll visualized by superposition of snapshots obtained under the existence of a single tracer particle in the cell. Images were obtained at the frequency $f = 12.5 \text{ Hz}$ and the acceleration $a = 50 \text{ m/s}^2$ with a cell with $W = 85 \text{ mm}$. (b) Width of downward flow developed near a side wall as a function of time, obtained from two cells with different widths $W = 55$ and 125 mm at the same f and a . (c) Superposition of snapshots in first 544 seconds for the cell with width 55 mm , visualizing the width of downward flow near the side wall. The dashed horizontal line indicates an average top surface of particles.

For later discussion, we here confirm experimentally that the width of downward flow developed near a side wall is comparable to the size of grain, which is consistent with the

previous report [5]. This is shown in Fig. 4 b quantifying the width of the downward flow near the wall. To obtain this plot, we took snapshots of a vibrated cell with a single tracer particle and superposed only a selected set of snapshots for a given duration, where we selected only the snapshots in which the particle moved down compared with its previous snapshot. An example of such superimposed snapshots is given in Fig. 4 c. We estimated the width from the maximum width as indicated in the figure. The width thus obtained are given as a function of time for two cells with different width in Fig. 4 b. As shown in the plot, the width saturates with time and the saturated value, which is several times of the grain size, is independent of the cell width.

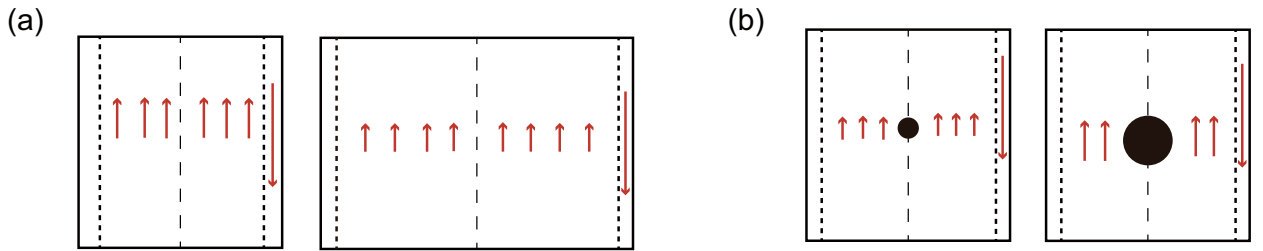


FIG. 5: (a) The effect of cell width on upward flow velocity. (b) The effect of intruder's diameter on upward flow velocity.

The independence of the width of the downward flow near the side wall from the cell width, confirmed in Fig. 4 b is physically natural because such a downward flow is caused by the friction effect near the side walls, and this effect should be the same for cells with different width as long as the side walls are well separated compared with the width of the downward flow. In addition, this implies that the flux of the downward flow is independent from the cell width W for a given v , and that the shear force which governs the flow is characterized not by v/W but by v/d .

Considering that the flow flux is conserved in the rolling motion, we expect that upwards velocity in the absence of the disk (and away from the disk) scales with a dimensionless factor d/W as illustrated in Fig. 5 a. However, alongside of the disk, it scales with $d/(W - D)$ as suggested in Fig. 5 b. In other words, there are two factors d/W and $d/(W - D)$, and both govern the rising velocity of the disk. Considering that the former is a decreasing function of W and the latter introduces a factor that increases with D , and expecting that the expression is independent of the smallest scale, the bead diameter d , a simplest possibility incorporating the two factors is a dimensionless factor D/W . This explains why U_2 scale

with D/W in Eq. (2).

This D dependence of U_2 is in contrast with results reported in the previous studies [5, 10]: they reported that the velocity of ascent due to convection is independent of the size of the intruder. This may be because the previous cases were more insensitive to the effect: they both considered not a two dimensional case as ours but a three-dimensional case, and they considered the cases in which the ratio of the intruder diameter to grain diameter are larger (the ratio is $\simeq 3.4 - 306$ in [5] and $\simeq 8 - 13$ in [10] while it is $\simeq 5 - 7$ in our case).

V. CONCLUSION

We examined the rising motion of an intruder in an original one-layer granular bed under continuous vibration for a wide range of parameters. We found that the motion was divided into two regimes and both regimes were well characterized by vibration velocity (v) through simple scaling laws. We provided physical interpretations based on convection and arch effect. Although two mechanisms are closely related, they can be clearly distinguished. The arch effect explains the scaling for the first regime ($\sim v^2$), while the convection mechanism explains the second scaling ($\sim v$). These two cases emphasize the importance of vibration velocity for understanding the BN effect. This generic feature of the BN effect confirmed in the present study will be useful not only in granular physics but also in many domain such as agriculture, and cosmetic or pharmaceutical industries [15, 16].

Acknowledgments

K. O. appreciates Mika Umehara (Ochanomizu University) for giving useful comments. This work was supported by JSPS KAKENHI Grant Number JP19H01859.

-
- [1] Harwood, C. F. Powder segregation due to vibration. *Powder Technology* **16**, 51–57 (1977).
 - [2] Williams, J. C. The segregation of particulate materials. a review. *Powder technology* **15**, 245–251 (1976).
 - [3] Rosato, A., Strandburg, K. J., Prinz, F. & Swendsen, R. H. Why the brazil nuts are on top: Size segregation of particulate matter by shaking. *Phys. Rev. Lett.* **58**, 1038–1040 (1987).

- [4] Clément, E., Duran, J. & Rajchenbach, J. Experimental study of heaping in a two-dimensional sand pile. *Physical Review Letters* **69**, 1189 (1992).
- [5] Knight, J. B., Jaeger, H. M. & Nagel, S. R. Vibration-induced size separation in granular media: The convection connection. *Phys. Rev. Lett.* **70**, 3728– (1993).
- [6] Duran, J., Rajchenbach, J. & Clement, E. Arching effect model for particle size segregation. *Phys. Rev. Lett.* **70**, 2431–2434 (1993).
- [7] Jullien, R., Meakin, P. & Pavlovitch, A. Three-dimensional model for particle-size segregation by shaking. *Phys. Rev. Lett.* **69**, 640 (1992).
- [8] Knight, J. B. *et al.* Experimental study of granular convection. *Physical Review E* **54**, 5726 (1996).
- [9] Vanel, L., Rosato, A. D. & Dave, R. N. Rise-time regimes of a large sphere in vibrated bulk solids. *Physical review letters* **78**, 1255 (1997).
- [10] Hejmady, P., Bandyopadhyay, R., Sabhapandit, S. & Dhar, A. Scaling behavior in the convection-driven brazil nut effect. *Phys. Rev. E* **86**, 050301(R) (2012).
- [11] Yamada, T. M. & Katsuragi, H. Scaling of convective velocity in a vertically vibrated granular bed. *Planetary and Space Science* **100**, 79–86 (2014).
- [12] Umehara, M. & Okumura, K. Rising obstacle in a two-dimensional granular bed induced by continuous and discontinuous vibrations: Dynamics governed by vibration velocity. *Journal of the Physical Society of Japan* **89**, 035001 (2020).
- [13] Ehrichs, E. *et al.* Granular convection observed by magnetic resonance imaging. *Science* **267**, 1632–1634 (1995).
- [14] Duran, J., Mazozi, T., Clément, E. & Rajchenbach, J. Size segregation in a two-dimensional sandpile: Convection and arching effects. *Physical Review E* **50**, 5138 (1994).
- [15] Duran, J. *Sables Poudres et Grains* (Editions Eyrolles in Paris, 1997).
- [16] Andreotti, B., Forterre, Y. & Pouliquen, O. *Granular media: between fluid and solid* (Cambridge University Press, 2013).